Polymer 49 (2008) 3136–3145

Contents lists available at ScienceDirect

Polymer

journal homepage: www.elsevier.com/locate/polymer

Torsion fatigue response of self-healing poly(dimethylsiloxane) elastomers

M.W. Keller [a,*], S.R. White [b], N.R. Sottos [c]

[a] University of Illinois at Urbana-Champaign, Beckman Institute for Advanced Science and Technology, Urbana, IL, United States
[b] University of Illinois at Urbana-Champaign, Department of Aerospace Engineering, Beckman Institute for Advanced Science and Technology, Urbana, IL, United States
[c] University of Illinois at Urbana-Champaign, Department of Materials Science and Engineering, Beckman Institute for Advanced Science and Technology, Urbana, IL, United States

ARTICLE INFO

Article history:
Received 31 January 2008
Received in revised form 14 April 2008
Accepted 15 April 2008
Available online 26 April 2008

Keywords:
Self-healing polymer
Elastomer
Fatigue

ABSTRACT

Incorporating self-healing functionality in a polysiloxane elastomer successfully retards the growth of fatigue cracks under torsional fatigue loading. The fully *in situ* self-healing material consists of a microencapsulated vinyl-terminated poly(dimethylsiloxane) resin containing platinum catalyst compounds and a microencapsulated initiator (methylhydrosiloxane), embedded in a poly(dimethylsiloxane) elastomer matrix. A torsion fatigue test protocol is adopted to assess the self-healing performance of two different elastomeric matrices. Significant recovery of torsional stiffness occurs after approximately 5 h, the time required to achieve a measurable degree of cure of the healing agents. Total fatigue crack growth in a self-healing specimen is reduced by 24% in comparison to relevant controls. The retardation of growing fatigue cracks is attributed, in part, to a sliding-crack-closure mechanism, where polymerized healing agent shields the crack tip from the applied far-field stress.

1. Introduction

Crack growth and damage accumulation generated by cyclic loading are traditionally addressed through the design of fatigue resistant structures and the application of external interventions, such as repair doubling [1]. Recent advances in self-healing materials [2,3] provide an alternative approach for mitigating fatigue damage. Self-healing materials possess the capability to autonomically repair quasi-static fracture damage [4–8] and to retard or even arrest fatigue crack growth [2,3,9].

Previous studies [2–4] of self-healing materials under fatigue loading focus on the dynamic repair of brittle, low strain-to-failure thermosetting epoxies by incorporation of the microcapsule-based healing system developed by White et al. [4]. The healing chemistry consists of microencapsulated dicyclopentadiene (DCPD) and a solid phase Grubbs' catalyst (benzylidene-bis(tricyclohexylphosphine)dichlororuthenium). Under certain conditions complete crack arrest is achieved [3]. The competition between the kinetic rates of chemical healing and mechanical damage dictates the degree to which growing fatigue cracks are healed [9]. Fatigue crack retardation and life extension in self-healing epoxy are achieved by several mechanisms. The inclusion of microcapsules in an epoxy matrix significantly reduces the crack growth rate, especially at high applied loads [10]. The polymerization of DCPD released from the capsules creates a wedge bonded between the faces of the propagating fatigue crack. This wedge significantly decreases the effective stress intensity factor (K_I^{eff}) and reduces the crack length. Prior to full polymerization, the viscous DCPD monomer introduces a secondary hydrodynamic shielding effect. Hydrodynamic shielding also reduces crack tip stress intensity, but is not as effective as the fully crosslinked polymer wedge [3].

In more recent work by Keller et al. [5], self-healing functionality is imparted to a poly(dimethylsiloxane) (PDMS) elastomer. Similar to the self-healing material system developed by White and coworkers [4], this elastomer utilizes a microcapsule-based healing mechanism. However, instead of the single microcapsule concept in previous systems, self-healing PDMS uses two types of liquid-filled capsules to provide self-healing functionality. These capsules contain the same initiator and resin material, encapsulated separately, as the matrix, resulting in a healing system that produces the same healed polymer as the surrounding matrix. Healing is initiated when a propagating crack ruptures microcapsules releasing their contents onto the crack plane. Capsule rupture can be achieved by both direct physical impingement or by significant triaxiality of the stress state near the crack tip. The fluids mix and polymerize, resulting in new PDMS that bonds to either side of the crack plane, healing the matrix. This self-healing elastomer routinely recovers between 70 and 100% of the original tear strength measured under quasi-static conditions. In this paper, we investigate the performance of the same self-healing poly(dimethylsiloxane) (PDMS) healing chemistry under dynamic fatigue loading.

The majority of research on the dynamic fatigue of elastomers and rubber focuses on the behavior of natural rubber, primarily

* Corresponding author. Present Address: The University of Tulsa, Department of Mechanical Engineering, Tulsa, OK, USA.
E-mail address: michael-keller@utulsa.edu (M.W. Keller).

0032-3861/$ – see front matter © 2008 Elsevier Ltd. All rights reserved.
doi:10.1016/j.polymer.2008.04.041

because of its commercial importance. Several review articles cover both the experimental and theoretical work characterizing the fatigue of rubber and other, synthetically produced, elastomers [11–13]. In the synthetic elastomer literature there are only a few publications that examine the fatigue performance of PDMS. Fitzgerald and coworkers have reported the effects of cyclic compression and shear stress on the elastic properties of a filled PDMS elastomer [14]. Savory et al. [15] evaluated the flexural fatigue of PDMS used in finger joint prostheses, but no data on the fatigue crack growth behavior, aside from cycles to failure, is presented. Fray and Altstädt compared the evolution of elastic properties of various copolymers with that of silicone rubber under a sustained load that increased stepwise [16].

Here, we introduce a torsion fatigue protocol commonly used by the tire industry to simulate fatigue cracking in the belt-edge region [17] to assess self-healing performance of PDMS under dynamic conditions. An extensive set of torsion fatigue experiments is carried out for two different PDMS matrices and are compared to appropriate control experiments.

2. Experimental

2.1. Torsion fatigue apparatus

Torsion fatigue experiments were conducted on a custom-built test apparatus adapted from the one constructed by De and Gent [18]. This test apparatus (Fig. 1a) was designed to allow the application of a small axial displacement (0.3 mm) to the torsion specimen in order to minimize friction effects. In addition, each of the pivot points was fitted with a ball bearing to minimize rotational friction. The guide bar (see Fig. 1a), required to prevent the hydraulic actuator from rotating, slides in a Derlin guide that was lubricated with a Teflon-based grease. The torsion mechanism was mounted on a servohydraulic test frame (Instron DynoMight 8841) fitted with a 250 N load cell. Test parameters were controlled via a computer connected to the load frame controller by an IEEE 488 bus.

This test apparatus enabled a linear servohydraulic test frame to generate a torsional deformation. Analysis of the test fixture was necessary to determine the moment M and angle of twist ϕ applied to the specimen for a given linear displacement. A schematic of a linkage in the fatigue fixture is shown in Fig. 1b. The two design parameters for the torsion fixture are the arm length l and the initial angle θ. For the experiments reported in this paper, $l = 102$ mm and $\theta = 45°$.

The geometric relationship between the angle of twist applied to the specimen ϕ and the applied linear displacement d of the arms is

$$\phi = 2\theta - 2\cos^{-1}\left(\cos\theta + \frac{d}{2l}\right). \quad (1)$$

For an applied linear force F, the moment M applied to the specimen is

$$M = Fl\left(\theta - \frac{\phi}{2}\right). \quad (2)$$

2.2. Sample preparation

Two elastomeric matrices are evaluated in this work: Sylgard 184 (Dow Corning), a highly compliant, commercially available addition cure PDMS, and RTV 630 (GE Silicones), another addition cure PDMS, but stiffer and more tear-resistant. Both matrix materials are supplied as two-part systems consisting of vinyl-terminated, high-molecular-weight liquid resins and liquid initiator materials. Platinum catalyst compounds are present in the resin materials and initiate a crosslinking reaction producing the elastomer. The healing chemistry consists of the matrix resin and initiator material for the Sylgard 184 PDMS material encapsulated in separate poly(urea–formaldehyde) microcapsules. These capsules are manufactured using the *in situ* microencapsulation procedure outlined by Brown et al. [19]. The initiator material is encapsulated as-received. Resin material is encapsulated with 20 wt% heptane to reduce the resin viscosity and improve capsule quality and yield.

Torsion fatigue specimens are manufactured by molding PDMS between two carbon steel grips that are treated with a primer (SS4155, GE Silicones). Both PDMS matrix materials are mixed in the recommended ratio of 10 parts resin to 1 part initiator and then degassed. Resin and initiator microcapsules are mechanically mixed into the matrix in the desired amounts and then degassed again. After pouring the uncured PDMS into the mold, the specimen is cured for 48 h at room temperature before testing. Final torsion specimens are circular cylinders 50 mm in diameter and 6.5 mm thick.

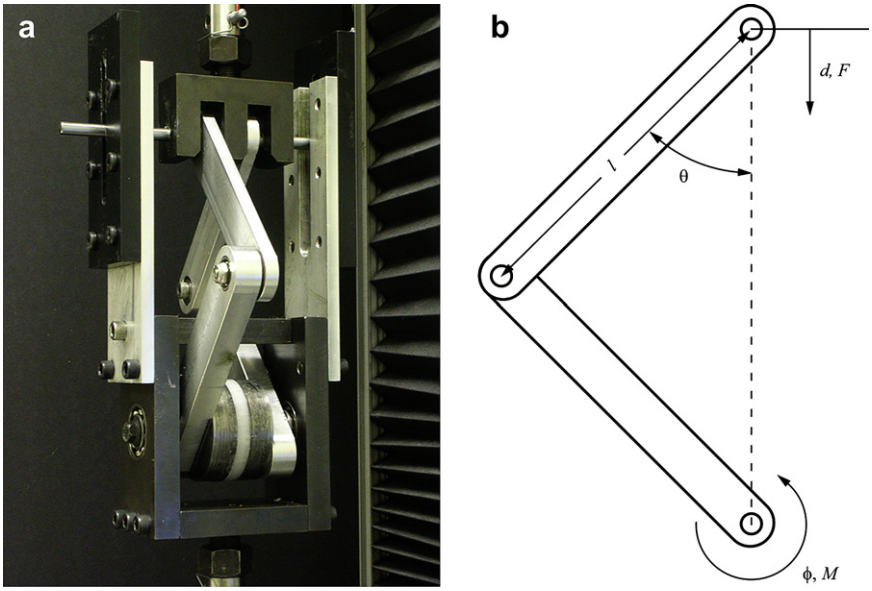

Fig. 1. (a) Photograph of the torsional fatigue test fixture, (b) schematic diagram of one of the torsion linkages.

The performance of two self-healing elastomers, differing only in the matrix material, was examined in this study. The Sylgard 184 PDMS matrix (used in previous quasi-static tear tests [5]) was highly compliant and had a tendency to debond from the sample grips during testing, making torsion testing difficult. The RTV 630 matrix was easier to bond to the grips, enabling more extensive measurements of fatigue crack growth. Four sample types were investigated for each matrix material including three separate controls and the fully *in situ* system. The sample types and compositions are listed in Table 1.

2.3. Test procedure and data analysis

The energy release rate and stiffness evolution of the torsional disk specimen have been analyzed previously in the literature [17,18,20,21] and are summarized in Appendix. Based on this analysis, the torsional stiffness of the specimen is expressed as a function of changing crack length [17],

$$K = \frac{M}{\phi} = \frac{\pi\mu}{2h}\left[R - a + \delta\left(1 - e^{-a/\delta}\right)\right]^4, \tag{3}$$

where M is the applied moment, ϕ is the applied twist, μ is the shear modulus of the material, δ is a correction factor, a is the crack length, R is the radius of the torsion specimen, and h is the specimen thickness. Fig. 2 shows a schematic of a torsion fatigue specimen. The correction factor δ is introduced to account for the contribution of surface-to-surface interactions to torsional stiffness. Both the characteristic shear modulus μ and correction factor δ are determined through calibration experiments. These experimentally calibrated values are then used in conjunction with Eq. (3) to track the crack length by measuring the change in the torsional stiffness of a specimen.

A circumferential pre-crack was introduced using a surgical scalpel mounted to the tool rest of a table-top lathe with manual screw feeds that permitted precise control of the pre-crack depth. After pre-cracking, the sample was mounted in the fatigue fixture and the test started. Fatigue testing was conducted in displacement control with the displacement applied using a sinusoid waveshape at a frequency of 2 Hz. The specimens were twisted through $\pm 6^\circ$ for 700,000 cycles. A fatigue cycle consisted of one full positive ($+6^\circ$) and one full negative (-6°) deformation excursion. This input was controlled to within 1.5% of the commanded deformation, minimizing any waveshape effects on fatigue performance. After the test was completed, the sample was removed from the test frame and was twisted to failure to examine the failure surface and to measure crack growth.

All fatigue samples exhibited an initial period of rapid decline in torsional stiffness. This decline has been reported previously [17,18] and is indicative of a crack tip conditioning period. The initial torsional stiffness was taken as the value just after this initial conditioning period. Specimens with a Sylgard matrix required a conditioning period of 20 cycles. Specimens with an RTV matrix required 500 cycles.

Table 1
Torsion fatigue sample types and composition (one sample at each capsule concentration)

Name	PDMS matrix material	Initiator capsule concentration (wt%)	Resin capsule concentration (wt%)
S-I	Sylgard 184	0	0
S-II	Sylgard 184	0	5
S-III	Sylgard 184	5	0
S-IV	Sylgard 184	5	5
R-I	RTV 630	0	0
R-II	RTV 630	0	10
R-III	RTV 630	5	0
R-IV	RTV 630	5	5

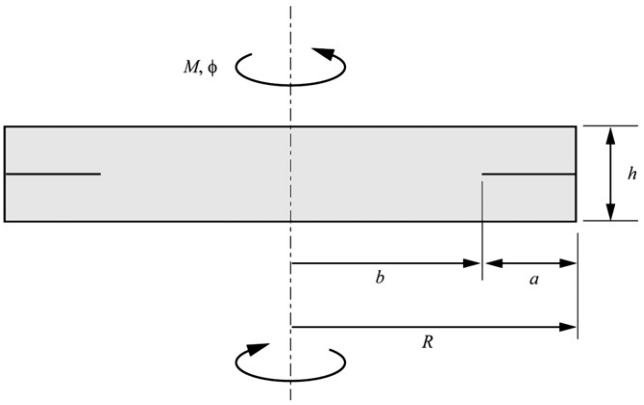

Fig. 2. Schematic of the cross-section of a torsion fatigue specimen.

3. Results

3.1. Sylgard 184 matrix

Torsion fatigue testing of the self-healing Sylgard 184 elastomer was performed for specimens with the compositions listed in Table 1. Poor adhesion to the sample grips limited the amount of fatigue testing with this matrix material. Additionally, a lack of well-defined morphology associated with the terminal length of the fatigue crack precluded accurate confirmation of the predicted crack lengths from the calibration. Therefore, fatigue data for the torsion testing of the Sylgard matrix specimens is presented as torsional stiffness evolution.

Fatigue crack growth of the Sylgard material proceeds rapidly, reaching stall in under 10 h (Fig. 3). Crack-stall phenomenon is a byproduct of this specimen geometry. As the crack propagates inward, the energy release rate G (Eq. (A.9)) reduces as a^{-2}, where a is the crack length, until the available energy is less than the critical energy to initiate fatigue growth [18].

Torsion fatigue behavior of the microcapsule-filled specimens is considerably different than that for the neat resin. Table 2 lists the measured initial and final torsional stiffnesses for each of the four

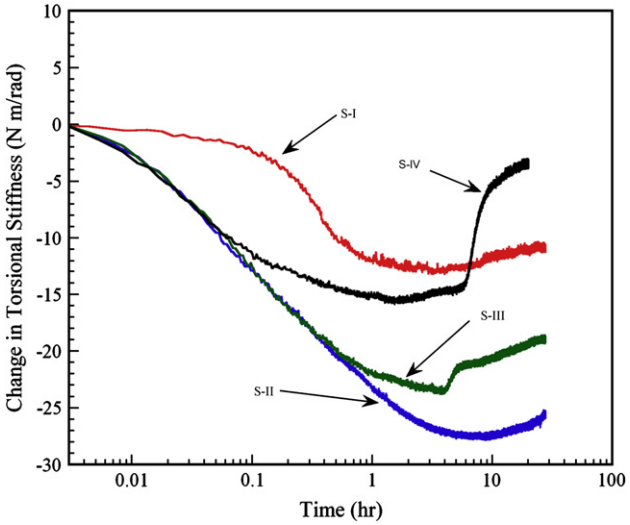

Fig. 3. Evolution of torsional stiffness during fatigue of Sylgard 184 matrix for neat resin (S-I), resin capsules (S-II), initiator capsules only (S-III), and *in situ* (S-IV) specimens.

Table 2
Measured initial (after 20 cycles) and final stiffnesses of Sylgard specimens (error estimated)

Specimen	Initial torsional stiffness (N m/rad)	Final torsional stiffness (N m/rad)
S-I	40.2 ± 0.2	29.5 ± 0.1
S-II	45.8 ± 0.2	20.4 ± 0.1
S-III	48.2 ± 0.2	29.1 ± 0.1
S-IV	33.7 ± 0.1	30.0 ± 0.1

Sylgard matrix specimens. Initial stiffness values vary from specimen to specimen and there are a number of potential causes. Torsional stiffness is dependent on crack length to the fourth power and small differences in pre-crack length will have large effects. The addition of microcapsules also alters the stiffness of a sample. However, dynamic mechanical analysis indicates that microcapsules generally stiffen the composite with increasing volume fraction [22], which is not necessarily reflected in the initial stiffness trends. Finally, there may be a lubrication effect from liquid resin released by microcapsules ruptured during the pre-cracking process.

Comparing the evolution of stiffness for each specimen as the test progresses (Fig. 3), the addition of microcapsules appears to have deleterious impact on the fatigue behavior. Microcapsule addition may cause a reduction of the matrix fatigue properties, or the lubrication effect from liquid resin released by ruptured microcapsules may influence fatigue performance. Previous studies on torsional fatigue [23,24] indicate that the surface–surface interactions during a test can significantly alter the apparent torsional stiffness of the specimen. Based on the behavior of the RTV matrix system presented in the next section and the quasi-static tear results in previous work [5], the stiffness reduction is most likely the result of lubrication. Further study is required to determine the exact mechanisms responsible for the torsional stiffness reduction.

Specimens that contain the initiator (S-III) or the initiator and resin (S-IV) exhibit a sharp increase of torsional stiffness at roughly 5 h. The elapsed time corresponds well to the gel time of the healing chemistry, implying that released healing agents are producing the stiffness increase. As observed previously in quasi-static testing, a measurable healing response is achieved with a specimen containing only initiator-filled microcapsules. The healing response for the initiator-only specimens is attributed to the interaction of the liberated initiator with residual vinyl functionality in the matrix, as well as initiator–initiator interactions [5]. Remarkably, the fully *in situ* specimen (S-IV) recovers almost all the original torsional stiffness of the material.

3.2. RTV 630 matrix material

Given the promising results achieved with the Sylgard system, we performed a comprehensive study of the RTV 630 elastomer. This elastomer is stiffer and has better adhesion to the steel fixtures when compared to Sylgard 184, greatly facilitating fatigue testing. As listed in Table 1, a range of control and self-healing samples was investigated.

3.2.1. Stiffness calibration

The relationship between the torsional stiffness of the neat RTV matrix and the crack length was determined by a series of torsion stiffness tests at known crack depths [17]. A pre-cut was precisely advanced in 1 mm steps using a scalpel mounted to a table-top lathe. Torsion load–displacement data were captured at each cut depth after the specimen had undergone 100 cycles of loading at the same rate and displacement as a fatigue test (2 Hz, ±6°). From these experiments, a master curve of torsional stiffness as a function of crack depth was constructed (Fig. 4). The characteristic shear modulus, $\mu = 1.23$ MPa, and the radius correction parameter, $\delta = 2.18$ mm, were extracted from the curve in Fig. 4 through a least-squares fit using Eq. (3). The characteristic shear modulus corresponds to a tensile Young's modulus of 3.7 MPa, close to the value of 3.5 MPa measured via dynamic mechanical analysis at 2 Hz for the RTV material [22].

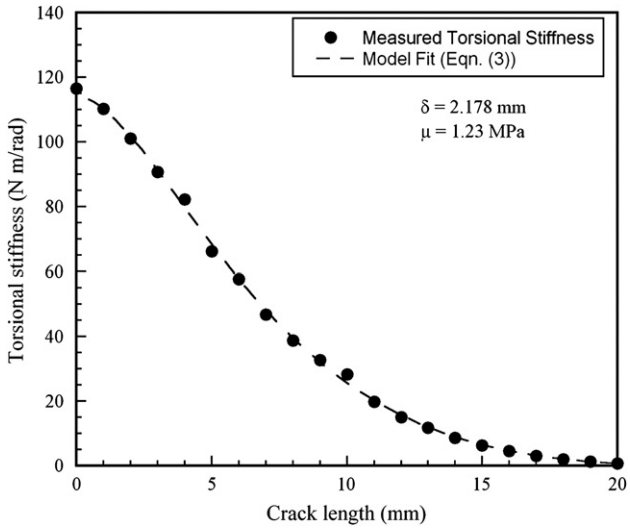

Fig. 4. Calibration of the specimen stiffness as a function of the crack depth for the RTV matrix. The dashed line is the predicted torsional stiffness from Eq. (3).

3.2.2. Torsion fatigue testing

The fully *in situ* self-healing performance of the RTV 630 was compared to three types of controls: material containing no microcapsules (neat) (R-I), material containing only resin microcapsules (R-II), and material containing only initiator microcapsules (R-III). Similar to the behavior of the Sylgard specimens described above, the initial torsional stiffnesses of each specimen were varied (Table 3). Since the microcapsule–PDMS composite generally exhibits a stiffer response than the PDMS matrix alone [22], the variation in initial stiffness is most likely a combination of initial crack-length differences and lubrication effects.

All of the samples with microcapsules (self-healing and controls) had greater terminal torsional stiffnesses when compared to the neat resin specimen (see Table 3). A 24% increase of the terminal torsional stiffness was achieved with the addition of 10 wt% resin microcapsules (R-II). Improved fatigue performance with the addition of microcapsules was also observed for microcapsule-filled epoxy [10]. As shown in the plot of stiffness evolution (Fig. 5), the neat resin sample (R-I) exhibited a slight increase in torsional stiffness near the beginning of the test. This increase was likely produced by frictional effects via surface-to-surface contact or surface interaction with debris generated by the fatigue crack propagation. Similar to the Sylgard material, the microcapsule-filled specimens also exhibit

Table 3
Measured initial (after 500 cycles) and final torsional stiffnesses for RTV specimens (error estimated)

Specimen	Initial torsional stiffness (N m/rad)	Final torsional stiffness (N m/rad)
R-I	90.9 ± 0.4	34.9 ± 0.1
R-II	94.3 ± 0.4	43.2 ± 0.2
R-III	91.6 ± 0.4	49.2 ± 0.2
R-IV	88.7 ± 0.4	53.8 ± 0.2

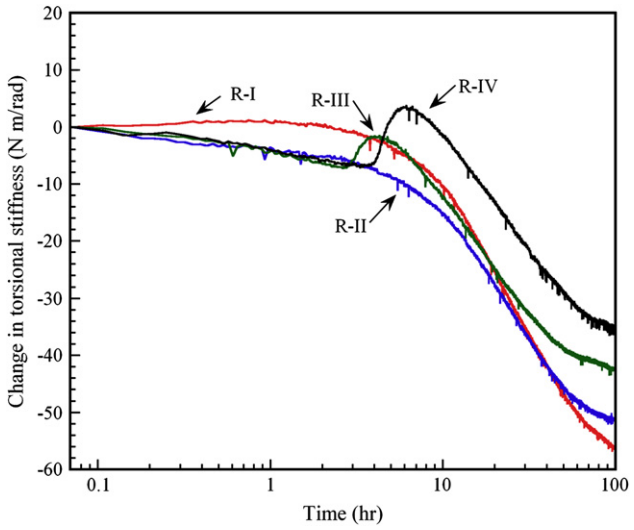

Fig. 5. Evolution of torsional stiffness during fatigue of RTV 630 matrix for neat resin (R-I), resin capsules only (R-II), initiator capsules only (R-III), and *in situ* (R-IV) specimens.

initially poorer fatigue performance, which is likely due to lubrication effects from liberated capsule contents.

Specimens containing only initiator microcapsules (R-III) exhibited a small increase in stiffness after 5 h of testing and a 41% increase in terminal stiffness over the neat resin. This behavior is consistent with that of the Sylgard specimens (S-III) in Fig. 3, indicating the initiator capsules induce a measurable self-healing effect. The fully *in situ* specimens (R-IV), which contained 5 wt% resin and 5 wt% initiator microcapsules, exhibited a 54% increase in terminal stiffness when compared to the neat resin (R-I) specimen. A marked increase in torsional stiffness also occurred at the same elapsed time as the Sylgard *in situ* specimen (S-IV). When compared to R-III, the onset of stiffness recovery occurred slightly later, behavior that was observed for the Sylgard matrix system as well (Fig. 3).

3.2.3. Crack growth measurement

The terminal crack length of each specimen was determined through direct measurement on the fracture surface at the end of a fatigue test. Photographs of fracture surfaces for each sample type are shown in Fig. 6. These samples were coated with a layer of Au/Pd for scanning electron microscopy (SEM) observation, which also improved contrast for photography. In each of the images, the smooth outer annulus corresponds to the pre-crack applied using a scalpel and lathe (zone 1). The rough inner annulus between the dotted and solid lines is the fatigue surface (zone 2). The center circle is the result of twisting the specimen to failure (after fatigue testing), indicated by a solid line of demarcation (zone 3). Measured terminal crack lengths for each specimen are summarized in Table 4. All samples exhibited asymmetric crack growth induced by small misalignments in the fatigue fixture. The total crack growth was

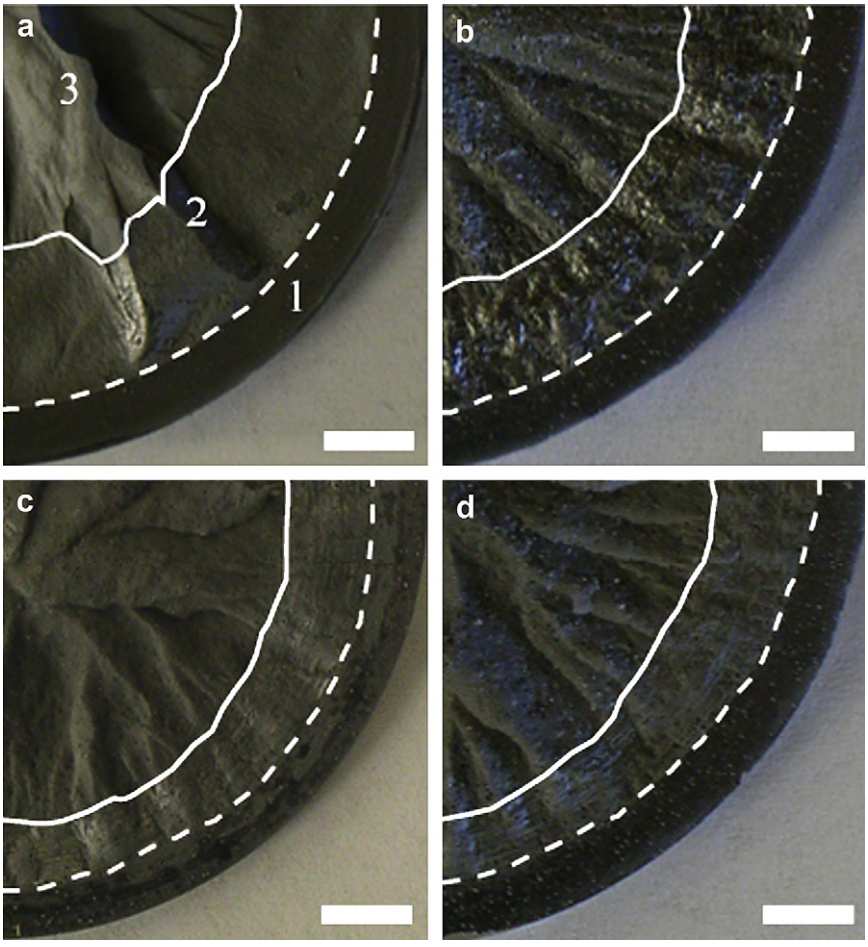

Fig. 6. Photographs of representative quadrants of failed torsion specimens for (a) neat RTV 630 resin (R-I), (b) 10 wt% resin microcapsules (R-II), (c) 5 wt% initiator microcapsules (R-III), and (d) *in situ* (R-IV). Dashed lines on the photographs indicate the edge of the pre-crack zone (zone 1). The solid lines indicate the terminal location of the fatigue crack (zone 2). Zone 3 is produced by the manual twist failure to separate the halves of the sample. The scale bars in each image represent 5 mm.

Table 4
Terminal crack lengths of RTV 630 torsion fatigue specimens

Specimen	Initiator capsule concentration (%)	Resin capsule concentration (%)	Terminal crack length (mm)	Reduction (%)
R-I	0	0	9.82 ± 0.01	0
R-II	5	0	8.91 ± 0.01	9
R-III	0	10	8.27 ± 0.01	16
R-IV	5	5	7.46 ± 0.01	24

Table 5
Comparison of terminal crack lengths predicted by Eq. (3) and measured values

Specimen	Predicted crack length (mm)	Actual crack length (mm)	Prediction error (%)
R-I	8.5	9.82 ± 0.01	13
R-II	7.5	8.91 ± 0.01	16
R-III	6.8	8.27 ± 0.01	18
R-IV	6.3	7.46 ± 0.01	15

calculated by measuring the distance between the edge of the specimen and the end of the fatigue crack (solid line) at 16 equiangular positions. These measurements were then averaged to determine the effective crack growth.

Based on the terminal crack growth measurements, the introduction of 10 wt% microcapsules reduced the terminal crack length by 9% when compared to specimen R-I. With active self-healing chemistry, specimen R-III, the terminal crack length was shortened by 16%. The fully *in situ* system reduced the terminal crack length by 24%.

In addition to allowing the measurement of the terminal crack lengths, the images in Fig. 6 also reveal several important macroscopic features of the crack surface. Neat RTV specimens (R-I, Fig. 6a) have large flat regions on the fracture surface, with only a few undulations, implying steady crack growth. Addition of microcapsules causes a striking change in this fracture morphology. The fracture surfaces of specimens with capsules contain prominent radial ridges, Fig. 6b–d. These ridges are reminiscent of rubber wear patterns first observed by Schallamach [25] and are indicative of frictional wear between the two crack faces. The macroscopic ridges are generally spaced 2–3 mm apart on the fatigue surface. At the edge of the specimen, assuming the maximal case of simple rigid-body motion, the crack faces move 2.6 mm relative to each other during twisting. A displacement of this distance implies that the ridges remain in their respective valleys during each twisting deformation.

3.2.4. Crack-length calculation

Crack-length evolution is calculated by fitting Eq. (3) to each data point using the values of μ and δ determined during the calibration experiment. The calculated crack length is shown in Fig. 7 as a function of time. These crack-length predictions are compared with the measured terminal crack lengths in Table 5 and measured pre-crack lengths in Table 6. For all specimens, Eq. (3) predicts both the terminal crack length and the pre-crack length within 20% of the experimental value. The under-prediction in both cases may arise from the morphology difference between the actual fatigue surfaces and the smooth cut of the calibration specimen. The smoother crack surface of the calibration specimen is associated with less crack-surface interactions, possibly leading to an underestimation of the correction parameter δ. In addition to the surface texture discrepancy, crack-length prediction can also be affected by variations in the modulus μ. As mentioned above, the incorporation of microcapsules does increase the elastic modulus [22]. However, since the prediction errors are similar for both the neat and microcapsule-filled specimens assuming the modulus value determined by the calibration experiment, the microcapsule effect on modulus does not appear to be a significant source of the prediction error.

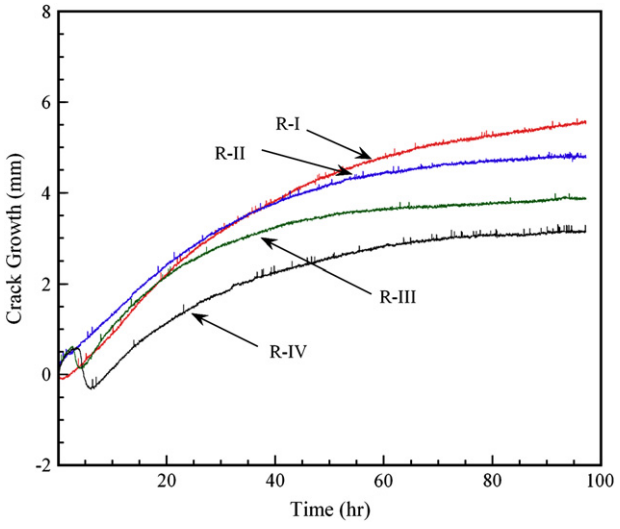

Fig. 7. Fatigue crack growth estimated from the calibration for the RTV 630 RTV 630 matrix for neat resin (R-I), resin capsules only (R-II), initiator capsules only (R-III), and *in situ* (R-IV) specimens.

Although there is some error in the predictions, the crack growth curves in Fig. 7 provide additional insight to the self-healing mechanisms. The control specimens R-I and R-II exhibit steady crack growth until reaching the stall depth. For specimens R-III and R-IV, however, the crack lengths exhibit a reversal corresponding to the increase in torsional stiffness in Fig. 5. Similar behavior occurs during the fatigue testing of self-healing epoxy [2,3] and is associated with a period of crack arrest as healing agent polymerizes and blunts the crack tip. The crack tip shielding effect from these reversal periods leads to significant extension of fatigue life in self-healing specimens.

3.3. Electron microscopy of fatigue surfaces

The morphology of the fatigue crack surfaces was examined by SEM to gain further insight into the mechanisms driving the stiffness recovery. The fatigue surface of the neat RTV material (R-I) was macroscopically smooth as shown in Fig. 8a. A higher magnification image of the fatigue surface, Fig. 8b, reveals a mostly featureless surface indicative of constant crack growth. In regions where macroscopic crack undulations occur (see Fig. 6a), there is evidence of wear such as grooving and surface striations. Additionally, there is a large amount of rolled debris on the fracture surface (Fig. 8c). This debris provides some evidence that the stiffness increase observed during the early stages of the fatigue test (Fig. 5) was generated by frictional interactions on the fatigue surface.

With the addition of microcapsules, periodically spaced ridges appear on the fatigue surface (Fig. 6b–d). This striking morphology

Table 6
Comparison of pre-crack lengths predicted by Eq. (3) and the measured values

Specimen	Predicted crack length (mm)	Actual crack length (mm)	Prediction error (%)
R-I	3.0	3.06 ± 0.01	3
R-II	2.7	3.08 ± 0.01	13
R-III	3.2	3.42 ± 0.01	7
R-IV	2.9	3.35 ± 0.01	13

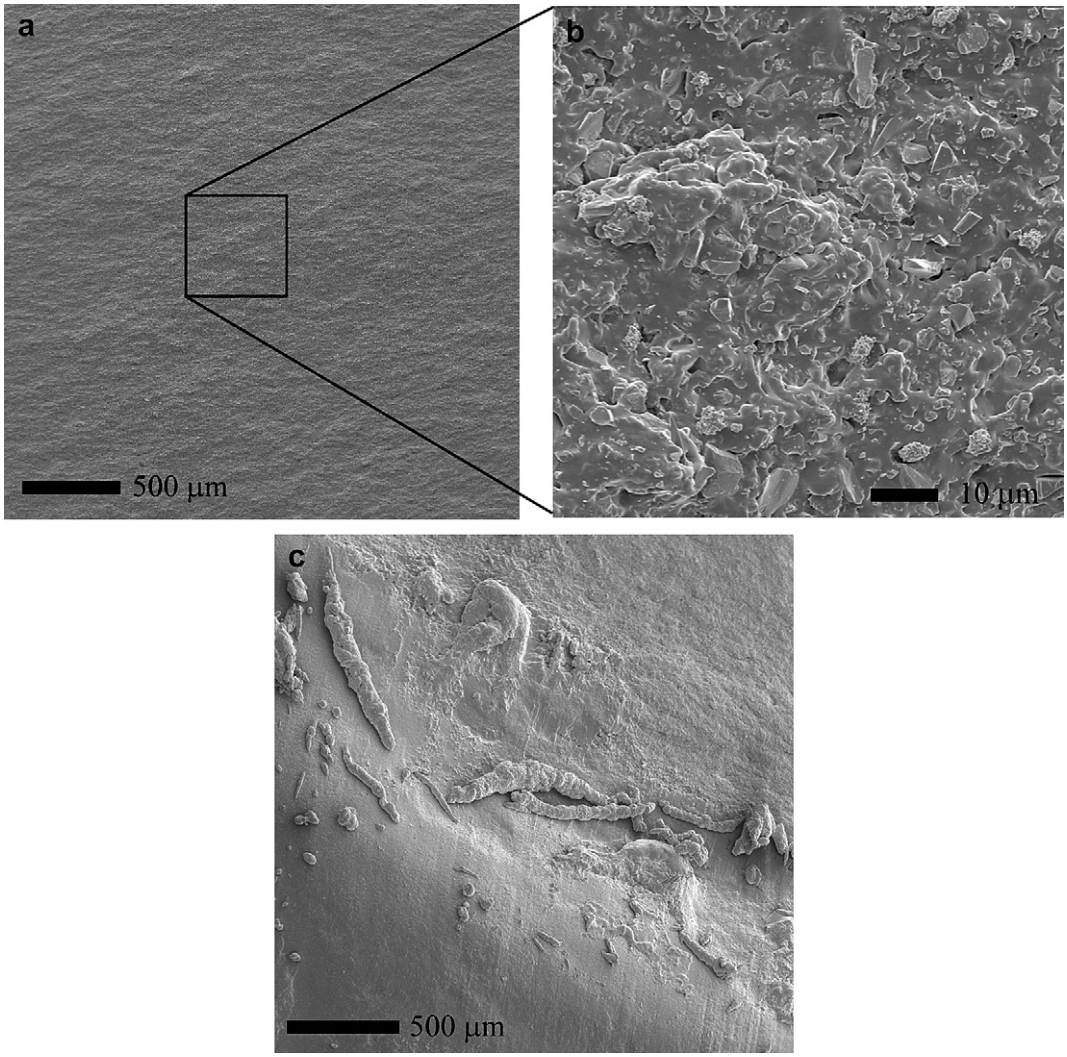

Fig. 8. Scanning electron microscope images of the fatigue surface of a neat (no microcapsules) RTV 630 torsion specimen (R-I). (a, b) The fatigue surface is generally smooth with little indication of surface wear. (c) When there are undulations, the matrix fails and introduces debris on the crack plane. The crack propagation is from left to right in all images.

change is not limited to macroscopic structures, but exists on the microscopic level as well. In the valleys of the periodic ridges, large regions of matrix damage are present (Fig. 9a). These regions have severe grooving and matrix erosion. Schallamach reports that the unidirectional abrasion of rubber generates ridges with peaks that eventually tear off [25]. The damage in the valleys of specimen R-II may be generated by a similar process driven by the contact between a ridge top and valley floor. In addition to the evidence of wear in the valleys, the leading edge of the raised ridges also exhibit wear patterns (Fig. 9b). These rough areas are characterized by small tongues of material projecting from the surface which are markers of frictional wear [26].

The fracture surface of an *in situ* specimen (R-IV) is similar to that for specimen R-II, but with more prominent wear patterns (Fig. 10a). The formation of new polymer in the crack plane during fatigue may increase the surface–surface interactions by bridging the gap created by the imposed axial separation. The healed polymer filling the crack plane may generate the observed increase in surface undercutting. Furthermore, the wear patterns such as those in Fig. 10b are spread over large portions of the fatigue surface, rather than just at the leading edge of ridges as observed for specimen R-II.

4. Discussion

Under quasi-static loading, healing efficiency is determined primarily by the strength of the adhesive bond between the polymerized healing agent and the crack faces. For fatigue loading, healing performance is influenced by more complex mechanisms. In prior studies of self-healing epoxy, the retardation of fatigue cracks is achieved through a combination of different mechanisms including hydrodynamic crack tip shielding, adhesive bonding, and artificial crack closure [2,3]. These same shielding mechanisms also play a role in the retardation of the propagating fatigue cracks in self-healing elastomers. In torsional fatigue another shielding mechanism is introduced based on frictional contact between the two crack faces that is induced and accentuated by healed polymer delivered to the crack plane.

Prior investigations on the torsion fatigue of steel indicate that surface interactions significantly affect the stress intensity at the crack tip [24]. The reduced crack growth rate observed in torsion fatigue tests is attributed to a dissipative mechanism known as "sliding-crack-closure" [23]. Sliding-crack-closure may account for the slightly improved fatigue response of specimen R-II. The ridge morphology observed for specimens containing microcapsules

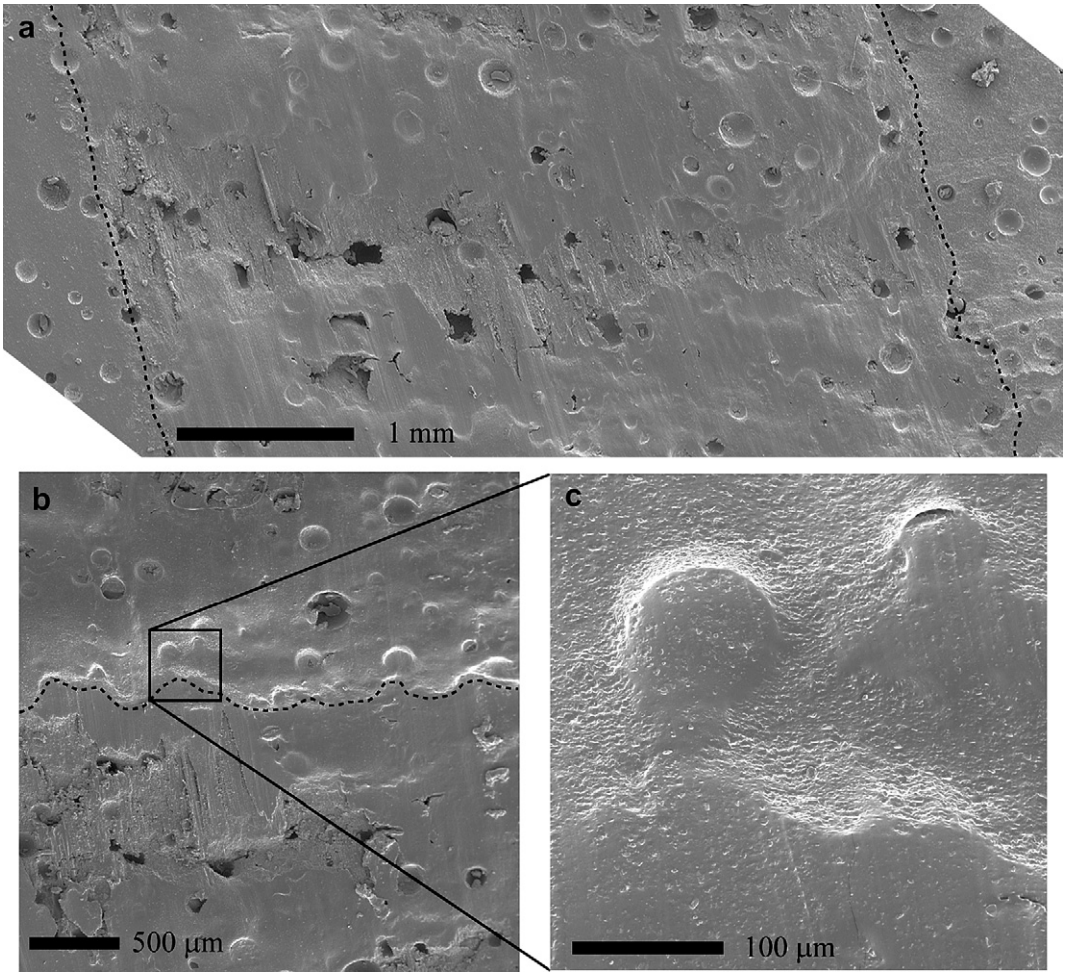

Fig. 9. Scanning electron microscope images of the fatigue surface specimen of RTV 630 containing 10 wt% resin microcapsules (R-II). Crack propagation is from left to right in all images. (a) Matrix failure due to abrasion during cyclic torsion. The dashed lines in (a) are the boundaries of the fatigue crack propagation zone. (b, c) Heavy frictional abrasion is generally limited to the leading edges of surface projections. The dashed line in (b) is the leading edge of a ridge.

produces a mutual-support phenomenon where adjacent ridges come into contact. For self-healing specimens, a second closure mechanism is introduced when the healing agent begins to polymerize. New polymer interacts with surface asperities on the crack faces to intensify the closure mechanism. This second mechanism produces the sharp increase in torsional stiffness observed for both the Sylgard and RTV matrix samples. Indications of strong frictional abrasion on the fatigue surfaces of the RTV specimens that contain active self-healing chemistry (Fig. 10) provide evidence of the crack-surface interactions generated by polymerized healing agent. The active generation of new polymer on the crack face in combination with the morphology-induced shielding mechanism reduce the apparent crack tip applied loading and slow crack propagation.

5. Conclusions

A torsion fatigue protocol was developed to assess the performance of self-healing elastomers under dynamic loading conditions. Evolution of torsional stiffness was measured for two different self-healing elastomers: a highly compliant Sylgard PDMS and a stiffer, more tear-resistant RTV 630 material. Significant recovery of torsional stiffness was observed for both materials. The time of recovery onset correlated with the bulk gel time of the healing chemistry, indicating that the increase in stiffness was generated through self-healing. Scanning electron microscopy revealed significant surface abrasion on the crack faces of the specimens containing active healing chemistry. These abrasions were associated with an operative "sliding-crack-closure" mechanism, which reduced the effective stress at the crack front and leads to the observed reduction of terminal crack length in the torsion fatigue specimens. For fully *in situ* specimens the action of the healing chemistry produced a 24% reduction in the total crack growth.

Acknowledgements

This work was supported in part by NASA through a subcontract with the Jet Propulsion Laboratory (JPL 1270900) and through the Air Force Office of Scientific Research. The authors would also like to thank Mr. David Stone for his efforts during the preliminary experimental testing. The electron microscopy was performed in the ITG facilities at the Beckman Institute.

Appendix. Torsion fatigue analysis

The energy release rates and stiffness evolution of torsion fatigue specimens were first analyzed by Aboutorabi and coworkers [20]. This analysis assumes that the material is linearly elastic in shear and that the specimen deformation is dominated by the uncracked portion of the disk. Consequently, the torsion stiffness K is expressed as

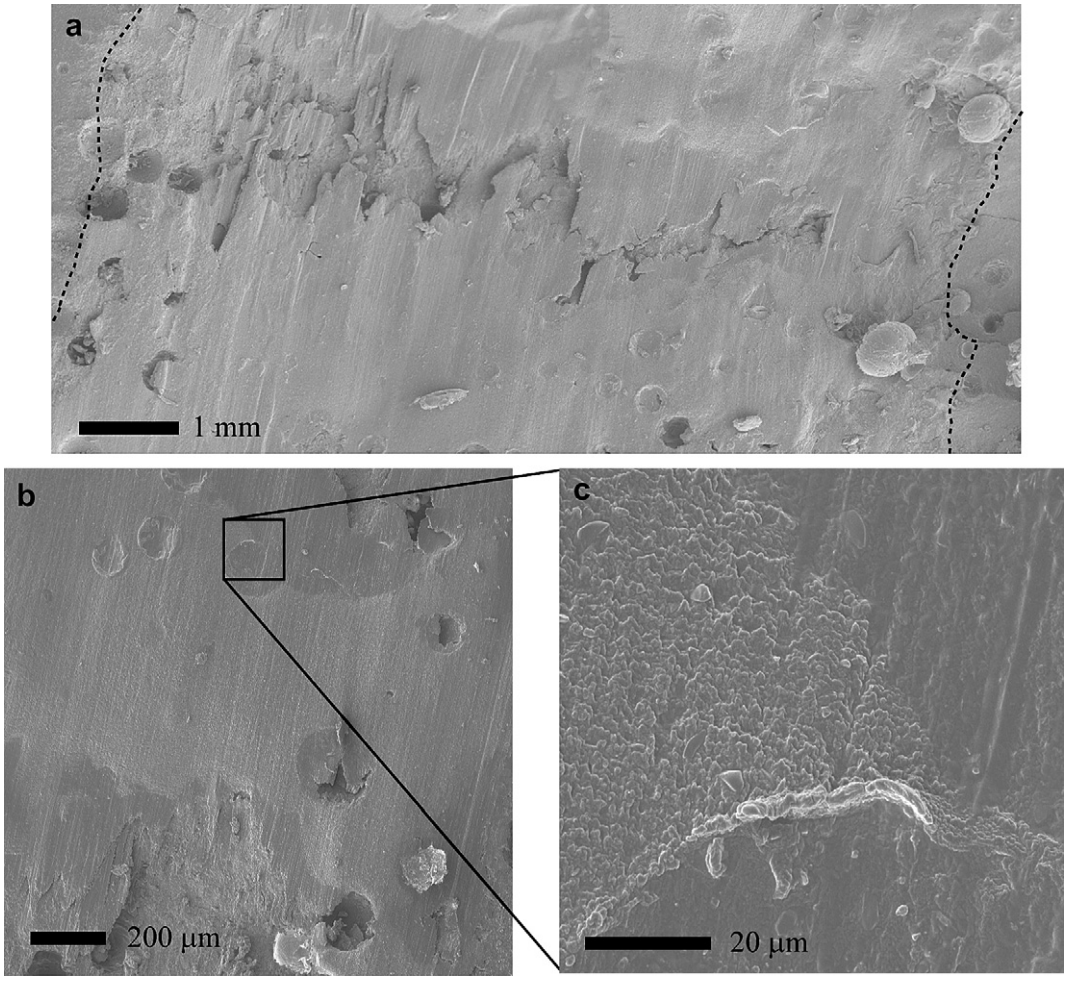

Fig. 10. Scanning electron microscope images of the fatigue surface specimen containing 5 wt% resin and 5 wt% initiator microcapsules (R-IV). Crack propagation is from left to right in all images. (a) Intense matrix failure on the floor of a valley. The dashed lines in (a) are the boundaries of the fatigue crack propagation zone. (b, c) Surface markings from frictional wear extend over large regions when compared to resin capsule only specimens (R-II).

$$K = \frac{M}{\phi} = \frac{\pi\mu}{2h}(R-a)^4, \tag{A.4}$$

where R is the disk radius, a is the crack length, M is the applied moment, ϕ is the angle of twist, h is the specimen thickness, and μ is the shear modulus. A schematic of the torsion fatigue specimen is shown in Fig. 2. Eq. (A.4) assumes that the uncracked portion of the disk carries all the stress in the specimen and that the cracked ligaments are unstressed. However, the cracked ligaments will carry some stress and this increases the apparent stiffness of the specimen. To account for this apparent increase, Aboutorabi and coworkers [20] introduced a correction factor δ to Eq. (A.4).

$$K = \frac{\pi\mu}{2h}(R+\delta-a)^4. \tag{A.5}$$

The correction factor acts to increase the apparent radius of the disk to account for the stress carried by the cracked ligaments. As $a \to 0$, the apparent radius of the disk will be larger than the actual specimen radius, an unphysical situation. Fleischman et al. [17] addressed this issue by introducing a correction factor that decays as the crack length approaches zero.

$$\delta_c = \delta\left(1 - e^{-a/\delta}\right). \tag{A.6}$$

Replacing δ in Eq. (A.5) with δ_c gives Eq. (3) above.

The energy release rate G for fixed boundary conditions and no external work is

$$G = -\left.\frac{\partial U}{\partial A}\right|_l, \tag{A.7}$$

where U is the total strain energy and A is the surface area of the crack. The strain energy is related to the effective stiffness K and twist angle θ by

$$U = \frac{1}{2}M\theta = \frac{1}{2}K\theta^2. \tag{A.8}$$

Eqs. (A.7) and (A.8) are combined and give a relationship between the torsional stiffness and energy release rate

$$G = \frac{\mu\theta^2}{2h(R-a)}\left[R - a + \delta\left(1 - e^{-a/\delta}\right)\right]^3\left[1 - e^{-a/\delta}\right]. \tag{A.9}$$

References

[1] Baker AA. Fatigue and Fracture of Engineering Materials and Structures 1993; 16(7):753–65.
[2] Brown EN, White SR, Sottos NR. Composites Science and Technology 2005; 65(15–16):2466–73.
[3] Brown EN, White SR, Sottos NR. Composites Science and Technology 2005; 65(15–16):2474–80.

[4] White SR, Sottos NR, Geubelle PH, Moore JS, Kessler MR, Sriram SR, et al. Nature 2001;409(6822):794–7.
[5] Keller MW, White SR, Sottos NR. Advanced Functional Materials 2007;17(14): 2399–404.
[6] Brown EN, Sottos NR, White SR. Experimental Mechanics 2002;42(4):372–9.
[7] Kessler MR, Sottos NR, White SR. Composites Part A – Applied Science and Manufacturing 2003;34(8):743–53.
[8] Kessler MR, White SR. Composites Part A – Applied Science and Manufacturing 2001;32(5):683–99.
[9] Jones AS, Rule JD, Moore JS, Sottos NR, White SR. Journal of the Royal Society Interface 2007;4:395–403.
[10] Brown EN, White SR, Sottos NR. Journal of Materials Science 2006;41(19): 6266–73.
[11] Mars WV, Fatemi A. International Journal of Fatigue 2002;24:949–61.
[12] Lake GJ. Rubber Chemistry and Technology 1995;68:435–60.
[13] Lake GJ. Progress of Rubber Technology 1983;45:89–143.
[14] Fitzgerald JJ, Martellock AC, Nielsen PL, Schillace RV. Polymer Engineering and Science 1992;32(18):1350–7.
[15] Savory KM, Hutchinson DT, Bloebaum R. Journal of Biomedical Materials Research 1994;28:1209–19.
[16] Fray ME, Altstädt V. Polymer 2003;44:4635–42.
[17] Fleischman TS, Kerchman V, Ebbot T. Tire Science and Technology 2001;29(2): 91–107.
[18] De DK, Gent AN. Rubber Chemistry and Technology 1998;71(1): 84–94.
[19] Brown EN, Kessler MR, Sottos NR, White SR. Journal of Microencapsulation 2003;20(6):719–30.
[20] Aboutorabi H, Ebbot T, Gent AN, Yeoh OH. Rubber Chemistry and Technology 1998;71(1):76–83.
[21] Gent AN, Yeoh OH. Rubber Chemistry and Technology 2003;76(5): 1276–89.
[22] Keller MW. A self-healing poly(dimethyl siloxane) elastomer. Ph.D. Dissertation, University of Illinois at Urbana-Champaign; 2007.
[23] Tschegg EK. Acta Metallurgica 1983;31:1323–30.
[24] Tschegg EK, Ritchie RO, McClintock FA. International Journal of Fatigue 1983;5: 29–35.
[25] Schallamach A. Transactions of the Institution of Rubber Industry 1952;28: 5823–37.
[26] Yang ACM, Ritchie RO, McClintock FA. Journal of Materials Science 1991;26: 5823–37.